International Journal of Electrical, Electronic and Communication Sciences
ISSN: 2517-9438
Vol:13, No:8, 2019

Modeling Thermo-Photo-Voltaic Selective Emitter Based on a Semi-Transparent Emitter with Integrated Narrow Band-Pass Pre-Filter

F. Stake

***Abstract*—**This work is a parametric study combining simple and well known optical theories. These simple theories are arranged to form part of one answer to the question: "Can a semi-transparent Thermo-Photo-Voltaic (TPV) emitter have an optical extinction spectrum so much greater than its optical absorption spectrum that it becomes its own band-pass pre-filter, and if so, how well might it be expected to suppress light of undesired wavelengths?" In the report, hypothetical materials and operating temperatures will be used for comparative analyses only. Thermal emission properties of these hypothetical materials were created using two openly available FORTRAN programs. Results indicate that if using highly transparent materials it may be possible to create a thermal emitter that is its own band-pass pre-filter.

***Keywords*—**Christensen effect, DISORT, index of refraction, scattering.

NOMENCLATURE

a	Particle Radius (length as specified or required for unit cancellation)
f_v	Fractional volume of continuous solid occupied by dispersed spheres
I	Intensity (Watts/m^2/μm)
k	Complex index of refraction
n	Real index of refraction
N_T	Number of dispersed spheres per unit volume of continuous phase
Q	Efficiency Factors
$W_{Black\ Body}$	Spectral Emissive Power of Blackbody (Watts/m^2/μm)
x	Sample thickness (cm)
α	Absorption coefficient (cm^{-1})
β	Extinction coefficient (cm^{-1})
θ	Angle relative to surface of emitter
κ	Absorption coefficient, particles and host (cm^{-1})
λ	Wavelength (length as specified or required for unit cancellation)
σ	Scattering Coefficient (cm^{-1})
τ	Optical Depth
ω	Single Scattering Albedo

A. Subscripts and Superscripts

abs	Absorption
c	Continuous (host)
d	Dispersed (particles)
sca	Scattering

Frank Stake is with the Drexel University, United States (e-mail: fstake@gmail.com).

I. THEORETICAL BACKGROUND

AN equation proposed by [1], shown as (1), is similar to the internal emission equation used in the standard radiative transfer equation. The key point is that emissive power of a semi-transparent body can be modeled as the Black Body Power at a given temperature times a scaling factor, and that scaling factor will geometrically approach unity as the product of thickness and absorption increase.

$$I_\lambda = n^2 \cdot \left(\frac{W_{Black\ Body,\lambda}}{\pi}\right) \cdot \left(1 - e^{\left(\frac{-\alpha_\lambda \cdot x}{\cos\theta}\right)}\right) \cdot \cos\theta \qquad (1)$$

Extinction is the sum of scattering and absorption, therefore keeping the magnitude of scattering so much greater than the magnitude of absorption (and corresponding emission) across most or all of the relevant light spectrum except the desired emission wavelengths that light at undesired wavelengths is reabsorbed at a rate that significantly diminishes its presence in the emission spectrum, is the key principle of a TPV selective emitter with integrated narrow band-pass filter. In (1), the author of [1] wrote the n term as constant rather than a function of wavelength; however that is only sometimes the case. In models run with the methodology in this paper, even considering highly transparent materials, the only models that could fulfill the goal of significantly diminishing emission of unwanted wavelengths relied in part on the indices of refraction of the host and dispersed scattering materials intersecting at the emission wavelength and diverging elsewhere, the Christensen effect.

Reference [2] proposed guidelines for when scattering by spheres dispersed in a continuous media may be considered independent of neighboring particles. When considering particles where the particle size (a) is very similar to the wavelength (λ, both in units of length), then to ensure independent scattering, the volume fraction of scattering spheres (f_v) must be kept low and a given maximum fraction of space occupied by spheres that would ensure independent scattering was 0.6%, although for systems where minimum inter-particle spacing and other considerations were maintained, higher fractional volumes may be possible while still maintaining independent scattering. It was hoped that this low volume fraction could apply to a random and unstructured dispersion of particles to simplify construction. It is possible that high volume fractions where scattering would enter the dependent scattering regime could also help create the desired condition, but the author was not aware of a definitive and

simple model for dependent scattering systems or close packed opal systems in the Mie scattering regime.

Reference [3] proposed a series of equations that describe the single scattering albedo (ω) of systems of independently scattering spheres of the same size, shown as (2).

$$N_T = \frac{3 \cdot f_v}{4 \cdot \pi \cdot a^3}$$
$$\kappa_\lambda = \alpha_\lambda^c \cdot (1 - f_v) + \pi \cdot a^2 \cdot N_T \cdot Q_{abs,\lambda}^d$$
$$\sigma_\lambda = \pi \cdot a^2 \cdot N_T \cdot Q_{sca,\lambda}^d \quad (2)$$
$$\beta_\lambda = \kappa_\lambda + \sigma_\lambda$$
$$\omega_\lambda = \frac{\sigma_\lambda}{\beta_\lambda}$$

Mie scattering and radiative transfers were computed using open source Fortran codes cited below. The only modification to these codes was the addition of loops to allow spectra to be produced. Mie scattering efficiency factors (Q) were calculated using a Mie scattering calculator titled "Homer.f" [4] run in GNU g77. Those spectra of Q were transformed by (2) to create spectra of ω and those ω spectra were input into DISORT (DIScrete Ordinate Radiative Transfer) [5], along with optical depth and wavelength data, and run in MinGW gfortran to create the product; emission spectra models.

II. Choice of Materials and Coefficients

Model emission spectra in this work will exclusively use two hypothetical materials, one with constant real and complex indices of refraction (n and k, respectively) and one with a k coefficient that sharply increases, thus causing a corresponding spike in n.

In the models, the k values of both materials were varied from 0.3 to 0.00003, as noted, except for a 0.2 μm wide spike in the k of the host material, which rose linearly to a value of 3 in all models, and n were set at 2.5 for the scattering particles and 1.5, except at the spike from 1.5 to 2.5 for the host medium, as shown in Fig. 1.

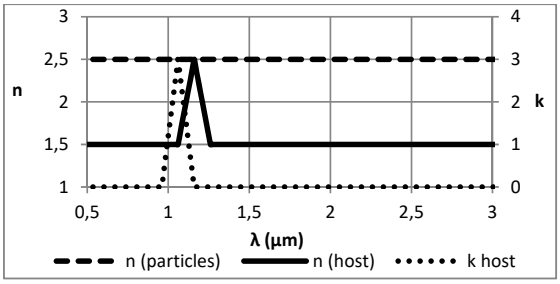

Fig. 1 Real and Complex indices of refraction used in models

Achieving a spike in the real refractive index would be the key that unlocks the possibility of using the Christiansen effect. Reference [6] proposed equations and guidelines for how increases and decreases in k would affect n. The shifts in index of refraction predicted by the Kramers-Kronig relations and [6] can be seen in various data; for example, [7] shows fundamentally similar peaks in the ultraviolet and infrared spectra of silica glass. Examples of similar spikes in n and k in the optical and near infrared are harder to find, but [8], [9] give examples where doping a thin film with metal nano-particles can change the real index of refraction on the order of 1 unit in the visible and near infrared regions; however, in general these specific materials are likely not suited for high temperature applications and have high k values, both attributes making them unsuitable for TPV. Still it lends hope to the possibility that suitable materials could be made.

Reference [6] had proposed a model for intra-band transitions of free carriers, where the change in n would be directly proportional to $1.38*N*10^{-21}$, where N would be the number of free carriers per cubic cm. Achieving carrier concentrations $\geq 10^{+21}$ should still be theoretically possible, although it may require "dopant" concentrations in the order of 10%. Again, the materials in this report are only hypothetical. There should also be some expectation that increased concentrations of "dopant" would lead to line broadening of any potential spikes in n or k. This would not necessarily be a problem, especially if low k values at wavelengths below the usable band gap of the photovoltaics were maintained.

In general, lower complex indices of refraction will allow for better scattering results. It is therefore notable that the changes in wavelength dependent complex index of refraction (and in turn the absorption coefficient in cm^{-1}) due to temperature in the semi-transparent dielectric solids are expected to be approximately one order of magnitude increase, geometrically increasing with temperature to the melting temperature of the material [10].

The operating temperature used in the models here was 2,500 Kelvin (Black Body peak emission at ~1.16 μm). The choice of temperature was completely arbitrary. Any temperature could have been used and would have followed the power outputs expected from the $W_{Black\ Body}$ term in (1). We should expect that in practice, the peak emission should be paired to a photovoltaic band gap, and that lower temperatures in general will lend themselves to materials that are easier to craft and, without special precautions, would tend to have longer operating lives. The models were assumed to have no heat losses and to have a uniform temperature; highly idealized and simplified assumptions.

Shockley-Queisser (S-Q) limits for the models were made for a single junction photovoltaic tuned to the peak of the emission spectra (1.16 μm, 1.068 eV). For reference a 2,500 K Black Body emitting to a photovoltaic with band gap at 1.068 eV would have an S-Q limit of 19.8%.

In the models considered, the radii of the scattering particles were 1.5 μm. This size was developed by rote comparison of oscillating ω curves produced by the Mie scattering calculator and (2), and using curves that produced consistently high ω values outside the emission wavelength. Using spheres of different sizes could be a practical way to help smooth out some of the oscillating curves produced by the Mie theory.

III. Results

In Figs. 2 and 3 models were run with extinction

coefficients for both the host (except at the k = 3 spike) and dispersion material as noted in the legends, and optical depths (τ) set at 100 for all wavelengths, and the theoretical slab modeled is on top of a Black Body emitter. From (1) and [1], a τ of about 3.5 will cause the scaling factor to approach unity and further increases in τ(x) will not significantly change the result. In Fig. 2, f_v was set at 0.6% and in Fig. 3, f_v was set at 6%. S-Q efficiencies are shown in Table I.

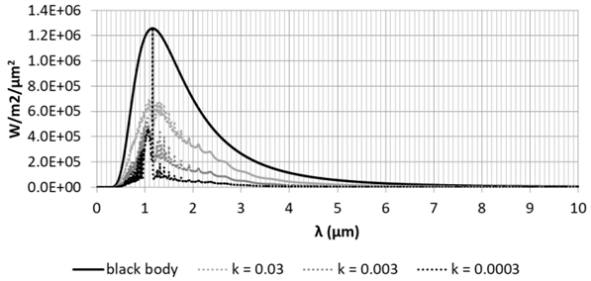

Fig. 2 Emission data for slabs with 0.6% scattering spheres and a constant optical depth of 100 at all wavelengths

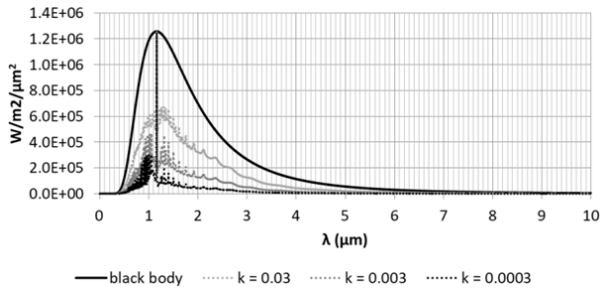

Fig. 3 Emission data for slabs with 6% scattering spheres and a constant optical depth of 100 at all wavelengths

TABLE I
SUMMARY S-Q LIMITS FOR MODELS IN FIGS. 2 AND 3

	k = 0.03	k = 0.003	k = 0.0003
f_v = 0.6%	**20.3%**	**24.8%**	**38.8%**
f_v = 6%	**19.6%**	**20.6%**	**25.8%**

One way to increase the S-Q efficiencies would be to lower the k value of the dispersed scattering media material. The models of Fig. 2 were re-calculated using a constant value of k = 0.00003 for the dispersed scattering media, and another model was added with the host media having k = 0.3 except at the k = 3 spike. This is shown in Fig. 4, while the S-Q limits are shown in Table II.

TABLE II
S-Q LIMITS FOR MODELS IN FIG. 2 RE-CALCULATED WITH K=0.00003 FOR ALL THREE MODELS

	k dispersion = 0.00003			
	k = 0.3	k = 0.03	k = 0.003	k = 0.0003
f_v = 0.6%	**28.3%**	**43.9%**	**55.9%**	**58.4%**

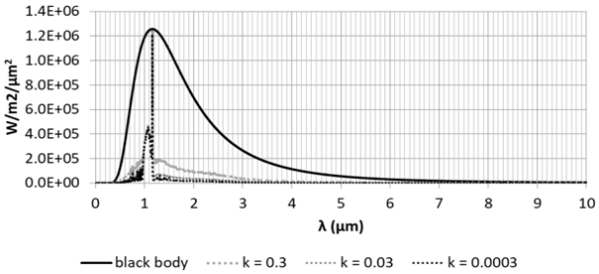

Fig. 4 Three of the four models noted in Table II with dispersed scattering media k=0.00003 for all models

An interesting observation is that if an isolated (no other radiation sources) and optically thick but low τ (τ << 3.5) slab were modeled the percent of energy at the peak would be much higher but the total power would be lower. For example if the optical depths of 10 μm slabs were modeled using a base k = 0.0003, any slab with the k =3 spike would have a sharp power spike where k was high, and for a model with scattering properties included the undesired wavelengths of radiation would be even more suppressed than in previous models. For a black body with no scattering and k equal to a constant 0.0003, the power curve would appear as a black body, but at a lower power and slightly misshapen due to k = 0.0003 having different α (cm^{-1}) values at different wavelengths. Using the ω coefficients from the k = 0.0003 model in Fig. 2, the S-Q limits for the three models described in this paragraph are presented in Table III and the models of a black body with no scattering and no spike in k, and a body with a spike in k and strong scattering are shown in Fig. 5. The third model was omitted for visual clarity in the Fig. 5.

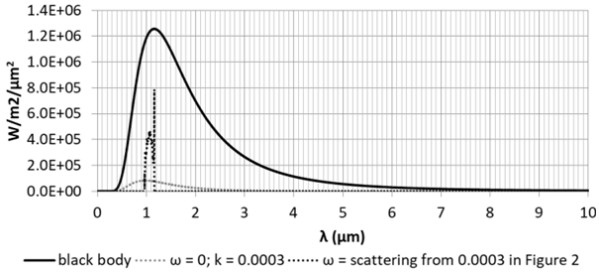

Fig. 5 Power for models of 10 μm isolated slabs, considering an emitter with spike in k and scattering, and a black body with no scattering

TABLE III
S-Q LIMITS FOR MODELS WHERE 10 MM ISOLATED SLABS WERE CONSIDERED

k = 0.0003	k = 0.0003 w/ spike to 3	k = 0.0003 w/ spike to 3
ω = 0	ω = 0	ω = scattering from 0.0003 model in Fig. 1
31.8%	**72.8%**	**91.7%**

Note that with the 10 μm slabs sitting on top of a black body substrate, the substrate would dominate. It should also be noted that for layers less than 10 μm, the effects would be more pronounced, but thin film effects would have to be considered. Thin film properties could potentially improve the

efficiency of the models but were not included here. For layers with the dispersed scattering particles, it is unclear how practically well the 3 μm diameter particles would fit into a 10 μm thick layer, especially at low fractional volumes; but for schemes with many repeating layers, it was hoped that the properties of the material as a whole would smooth over variations in individual layers.

One way to enhance the S-Q efficiency of a slab might be to have low τ alternating layers of scattering and non-scattering material, where the non-scattering layers were made of the material with the higher n value and where scattering could cause unwanted photons to enter non-scattering layers at angles, thus being trapped due to total internal refraction. This is shown schematically in Fig. 6, both as a pure concept (left) and as equivalent data that was input into DISORT (right). The model was run with 1,000 alternating pairs of layers (2,000 10 μm layers as described in the schematic on the left hand side of Fig. 6 or 5,000 layers used in the DISORT model). More layers were not considered due to limitations in the program in the form used. The energy captured by total internal refraction in each of the non-scattering layers was modeled by adding a non-emitting and non-scattering layer with an optical depth that would be proportional to the critical angle divided by a right angle, shown in (3) and the right and side of Fig. 6.

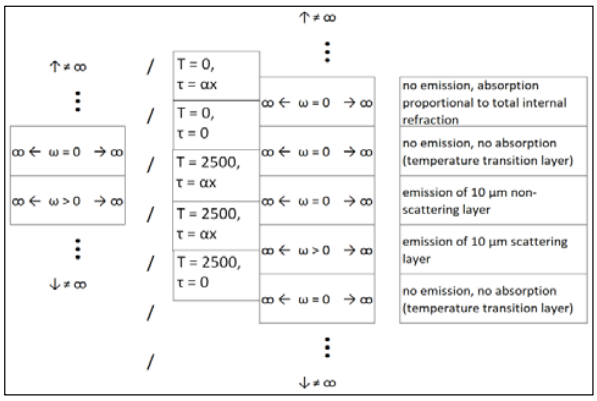

Fig. 6 Schematic of alternating layers (left) and Schematic of alternating layers as represented in DISORT model

$$\tau = \ln\left(\frac{\frac{\pi}{2}}{\sin^{-1}\left(\frac{n_c}{n_d}\right)}\right) \quad (3)$$

Two models are shown in Fig. 7, based on the 1,000 alternating layers scheme described above and in (3) and Fig. 6. Both models had f_v = 0.6%. One used the k = 0.0003 material in Fig. 2 which had a S-Q limit efficiency of 38.8%, and the other was based on the k = 0.3 material from Fig. 4 that had an S-Q limit efficiency of 28.3%. These models run as 1,000 alternating pairs of 10 μm layers had S-Q limit efficiencies boosted to 92.2% and 37.5%, respectively. In both cases, the absorptive τ(x) of the bulk models was thick enough that increases in the thickness or the model being placed on top of a black body emitter would not significantly change the resulting emission.

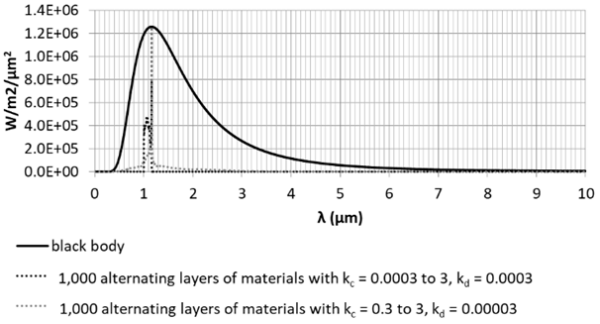

Fig. 7 Output of models of 1,000 alternating layers as described in Fig. 6, and assuming some total internal refraction by the layers of non-scattering, high n material as described by (3)

IV. Conclusion

The relatively short and broad spikes on the shorter wavelength side of the 1.16 μm peak that become prominent in Figs. 5 and 7 are likely due to oscillations in the ω spectra produced by the Mie theory. In practice, we should expect those peaks would merge and broaden for several practical reasons that could not be modeled in this work. That is not necessarily a problem, as long as the peaks in the usable spectrum are large and radiation in the unusable parts of the spectrum are suppressed.

The techniques used in this report can work with other techniques. The dopants and wavelength scale particles used to spike the k value could potentially boost selective emission, and models here were based on black body emitters, not selective grey body emitters. Other techniques such as close packing of spheres and spheres with a distribution of sizes could help increase scattering efficiency. Tuned multi-junction photovoltaic and thin film band-pass reflectors in or on the emitter and photovoltaic could further enhance efficiency.

This concludes an exercise designed to show that it may be possible to create a bulk material where the optical extinction spectrum is so much greater than the optical absorption spectrum that it becomes its own band-pass pre-filter, thus helping boost TPV efficiency.

References

[1] Gardon, R., The Emissivity of Transparent Materials. *Journal of the American Ceramic Society*. 39(8):278-287; 1956.
[2] Tien, C. L., Drolen, B. L., Thermal radiation in particulate media with dependent and independent scattering. *Annual review of numerical fluid mechanics and heat transfer*. Volume 1 (A88-18971 06-34). Washington, DC, Hemisphere Publishing Corp, p. 1-32; 1987.
[3] Pilon, L., Viskanta R. Radiation Characteristics of Glass Containing Gas Bubbles. *Journal of the American Ceramic Society*, Vol.86, No.8, pp.1313-1320.; 2003.
[4] Quirantes, A., Homer.f Mie Scattering Calculator (software) (2003), http://www.ugr.es/~aquiran/codigos.htm.
[5] Wiscombe, W., Stamnes, K., Tsay, S., Laszlo, I., DISORT 2.0 BETA (software) (2008).
[6] Stern, F., Dispersion of the Index of Refraction Near the Absorption Edge of Semiconductors. *Physical Review* Volume I33, Number 6a 16 March 1964.
[7] Kitamura, R., Pilon, L., Jonasz, M., Optical constants of silica glass from extreme ultraviolet to far infrared at near room temperature.

Applied Optics. Vol. 46, No. 33 pp 8118-8133. November 2007.
[8] Gültekin, A., Effect of Au Nanoparticles Doping on The Properties of TiO2 Thin Films. *Materials Science (Medžiagotyra)*. Vol. 20, No. 1. 2014.
[9] Hussain, Z., Dopant-dependent reflectivity and refractive index of microcrystalline HxWO3 and LixWO3 bronze thin films. *Applied Optics*. Vol. 41, No. 31. 1 November 2002.
[10] Thomas, M. E., Temperature Dependence of the Complex Index of Refraction in Handbook of Optical Constants of Solids. Volume 2, edited by Palik, E. Academic Press; 1991.